# Chemical Vapor Deposition of N-Doped Graphene and Carbon Films: The Role of Precursors and Gas Phase

**Yoshikazu Ito,[†] Christos Christodoulou,[‡] Marco Vittorio Nardi,[‡] Norbert Koch,[‡] Hermann Sachdev,[†,*] and Klaus Müllen[†,*]**

[†]Synthetic Chemistry, Max-Planck-Institute for Polymer Research, Ackermannweg 10, 55128 Mainz, Germany and [‡]Institut für Physik & IRIS Adlershof, Humboldt-Universität zu Berlin, Brook-Taylor-Straße 6, 12489 Berlin, Germany

**ABSTRACT** Thermally induced chemical vapor deposition (CVD) was used to study the formation of nitrogen-doped graphene and carbon films on copper from aliphatic nitrogen-containing precursors consisting of $C_1$- and $C_2$-units and (hetero)aromatic nitrogen-containing ring systems. The structure and quality of the resulting films were correlated to the influence of the functional groups of the precursor molecules and gas phase composition. They were analyzed with SEM, TEM, EDX, XPS, and Raman spectroscopy. The presence of (N-doped) graphene was confirmed by the 2D mode of the Raman spectra. The isolated graphene films obtained from nitrogen-containing precursors reveal a high conductivity and transparency compared to standard graphene CVD samples. Precursors with amine functional groups (*e.g.*, methylamine) can lead to a direct formation of graphene even without additional hydrogen present in the gas phase. This is not observed for, *e.g.*, methane under comparable CVD conditions. Therefore, the intermediate gas phase species (*e.g.*, amine radicals) can significantly enhance the graphene film growth kinetics. Kinetic and thermodynamic effects can be invoked to discuss the decay of the precursors.

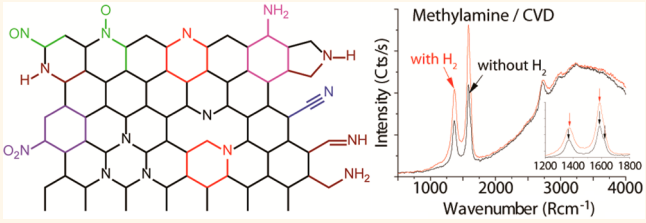


**KEYWORDS:** CVD · graphene · N-doping · formation mechanism · precursor chemistry · Raman spectroscopy

The deposition of carbon films from the gas phase leads to materials of widely different structure and composition. The films can be (i) crystalline, *e.g.*, like graphene, graphite or diamond, and consist ideally of a single type of either $sp^2$ or $sp^3$ hybridized carbon atoms, (ii) can contain domains of any of these phases in more or less ordered arrangements, or (iii) can even incorporate a considerable amount of hydrogen or other heteroatoms. Within this manifold of carbon films, graphene, a two-dimensional allotrope of carbon has recently attained high interest due to its electronic and optical properties and chemical inertness.[1−3] Graphene with controllable electronic properties is expected to be a promising material for the development of new electronic devices,[4,5] such as, *e.g.*, field-effect transistors[6] or electrochemical sensors,[7,8] as well as for applications in energy storage[9,10] and conversion systems like super capacitors,[11] lithium batteries,[12] and fuel cells.[13] Furthermore, transparent conducting graphene films are considered for organic electronic devices such as OLED's and organic solar cells.[14] Graphene itself does not reveal a band gap and therefore has no intrinsic semiconducting properties. Thus, doping of graphene with hetero-elements like boron (B) or nitrogen (N), which fit into the carbon lattice, is an important issue. Theoretical and experimental studies indicate that B- or N-doped graphenes reveal p- or n-type semiconductor characteristics[15−17] accompanied by a band gap opening[18−20] and thus doped graphene and structurally related graphene nanoribbons are considered as promising materials with tunable electronic properties.[21,22]

N-Doped graphene, and particularly B-doped graphene, are still scarcely investigated experimentally as compared to graphene[23] and graphene oxide.[24] So far, few methods for generating N-doped graphene are described. Among these are thermal CVD of methane and ammonia gas,[25] CVD of molecular precursors like pyridine[26] or acetonitrile[27] on a Cu substrate or exposure of graphene to a nitrogen[28] or

* Address correspondence to sachdev@mpip-mainz.mpg.de, muellen@mpip-mainz.mpg.de.

Received for review October 30, 2013 and accepted March 18, 2014.

**Published online March 18, 2014**
**10.1021/nn405661b**

ammonia[29] containing plasma discharge. In these reactions, the presence of nitrogen was identified by XPS, whereas the mechanism for nitrogen incorporation at specific positions of the graphene lattice is still not understood.[15,16,30] Recently, the formation mechanism of graphene from molecular precursors has been investigated. From the decay it was reasoned that dicarbon ($C_2$-) species, formed as reaction intermediates, can contribute significantly to the built-up of graphene.[31] Since the formation of the graphene lattice will not be accomplished by methane as a $C_1$- carbon source directly, the intermediate species generated during the precursor decay determine the quality of the newly formed graphene or carbon materials from the gas phase.

Here it was investigated whether the nature of the precursor substituents and the gas phase composition determines the quality of the obtained carbon films. Precursors with $C_1$- (methane, methylamine, nitromethane) or $C_2$- (ethylamine, ethanolamine, nitroethane, acetonitrile) units as well as (hetero)aromatic ring systems (benzene, pyridine, aniline, nitrobenzene) were separately deposited with and without additional hydrogen in the gas phase to investigate the nitrogen incorporation into carbon films and the formation of graphene. We consequently compared higher aliphatic amines (ethylamine $C_2H_5-NH_2$, ethanolamine $HO-C_2H_4-NH_2$), aliphatic nitro compounds with $C_1$- and $C_2$- building blocks (nitromethane $CH_3-NO_2$, nitroethane $C_2H_5-NO_2$) and nitriles (acetonitrile $CH_3-CN$) with appropriate (hetero)aromatic counterparts like benzene (as a reference), aniline ($C_6H_5-NH_2$), nitrobenzene ($C_6H_5-NO_2$), and pyridine ($C_5H_5N$). Each of these precursors serves as a model for the higher homologues, the basic reactivity of the functional groups has been elucidated here.

Therefore, the CVD of nitrogen-containing precursors with those different functional groups was performed. A schematic overview of the precursors is given in Figure 1.

The precursor decomposition was performed at different CVD temperatures with or without additional hydrogen during the CVD process. The deposited films were characterized by SEM, EDX, TEM, and Raman spectroscopy, which allows distinguishing between carbon films in general and graphene films with an evident presence of the 2D mode. In addition, isolated graphene films were transferred onto glass substrates, and optical transparencies as well as surface conductivity were measured.

## RESULTS AND DISCUSSION

The thermally induced CVD experiments were conducted with a representative set of precursors depicted in Figure 1 in a hot wall CVD reactor with a precursor

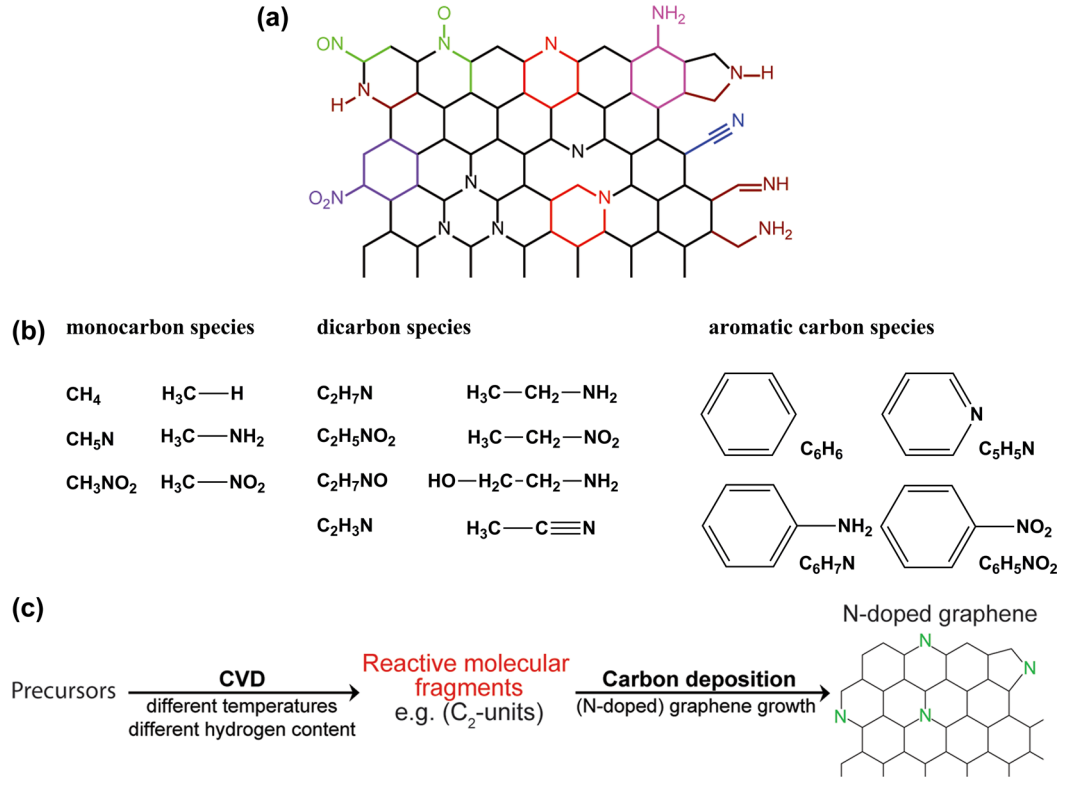


**Figure 1. (a) Potential nitrogen functions present in N-doped carbon materials, *e.g.*, for N-doped graphene. (b) CVD precursors with different functional groups as used in this study: *e.g.*, aliphatic nitrogen compounds with $C_1$- and $C_2$- carbon fragments and (hetero)aromatic precursors containing nitrogen in different oxidization states. The CVD of methane, methylamine, ethylamine, ethanol amine, nitromethane, nitroethane, acetonitrile, pyridine, aniline, nitrobenzene, and benzene was performed in this study. (c) Schematic formation of nitrogen-containing graphene by CVD.**

**TABLE 1. Peak Positions and Line Widths (in $cm^{-1}$) of the Raman D, G, and D′ Bands, Intensity Ratios of D and G Peaks for (N-Doped) Graphene and Carbon Films Grown on Copper Substrates with or without Additional Hydrogen during CVD (Excitation: 488 nm, Power: 2 mW)**

| modes (fwhm) | D band (fwhm) | G band (fwhm) | D′ band (fwhm) | 2D band (fwhm) | $I_D/I_G$ | $I_{2D}/I_G$ | $I_{D'}/I_G$ | $I_{2D}/I_{D'}$ |
|---|---|---|---|---|---|---|---|---|
| methane $H_2$ | – (–) | 1584 (14) | – (–) | 2714 (20) | – | 3.70 | – | – |
| no $H_2$ | 1355 (60) | 1588 (50) | – (–) | – (–) | 0.60 | – | – | – |
| methylamine $H_2$ | 1370 (33) | 1588 (25) | 1622 (12) | 2720 (40) | 0.79 | 0.58 | 0.09 | 6.5 |
| no $H_2$ | 1372 (46) | 1588 (29) | 1620 (18) | 2729 (55) | 0.90 | 0.36 | 0.10 | 3.7 |
| ethylamine $H_2$ | 1376 (40) | 1592.5 (20) | 1630 (18) | 2741 (41) | 0.93 | 0.90 | 0.15 | 5.7 |
| no $H_2$ | 1376 (60) | 1592 (30) | 1630 (30) | 2741 (55) | 1.50 | 0.48 | 0.21 | 2.3 |
| ethanolamine $H_2$ | 1367.5 (32) | 1585.5 (19) | 1625 (17) | 2729.5 (52) | 0.76 | 1.20 | 0.10 | 10 |
| no $H_2$ | 1366 (34) | 1593 (23) | 1630 (10) | 2720 (38) | 0.61 | 0.67 | 0.03 | 22 |
| nitromethane $H_2$ | – (–) | – (–) | – (–) | – (–) | – | – | – | – |
| no $H_2$ | 1368 (19) | 1602 (55) | – (–) | – (–) | 0.63 | – | – | – |
| nitroethane $H_2$ | – (–) | – (–) | – (–) | – (–) | – | – | – | – |
| no $H_2$ | – (–) | – (–) | – (–) | – (–) | – | – | – | – |
| acetonitrile $H_2$ | 1369 (19) | 1595 (16) | 1634 (8) | 2715 (22) | 0.74 | 2.8 | 0.11 | 25 |
| no $H_2$ | 1371 (21) | 1598 (18) | 1634 (9) | 2735 (38) | 1.40 | 1.4 | 0.18 | 7.7 |
| pyridine $H_2$ | 1365.5 (19) | 1599 (13) | 1645 (10) | 2721 (23) | 0.46 | 3.5 | 0.036 | 111 |
| no $H_2$ | 1375 (150) | 1596 (80) | – (–) | – (–) | 1.60 | – | – | – |
| aniline $H_2$ | 1370 (70) | 1587 (18) | 1630 (35) | 2731 (32) | 1.70 | 0.78 | 0.41 | 1.9 |
| no $H_2$ | 1378 (150) | 1600 (70) | – (–) | – (–) | 2.1 | – | – | – |
| nitrobenzene $H_2$ | 1366 (20) | 1588 (14) | 1635 (13) | 2723 (28) | 0.36 | 1.60 | 0.054 | 85 |
| no $H_2$ | 1378 (140) | 1602 (65) | – (–) | – (–) | 2.20 | – | – | – |
| benzene $H_2$ | 1354 (20) | 1585 (15) | 1618 (5) | 2700 (19) | 0.32 | 3.60 | 0.016 | 222 |
| no $H_2$ | 1378 (150) | 1602 (60) | – (–) | – (–) | 2.7 | – | – | – |

inlet system according to a time–temperature–gas flow profile depicted in the Supporting Information. The precursors are listed in Table 1. $C_1$- and $C_2$- species as well as (hetero)aromatic building blocks were screened for their ability to form graphene and nitrogen-doped graphene films. Whereas mobile molecular $C_2$- building blocks are discussed in the literature to play a dominant role in the formation of the graphene lattice,[31] $C_1$- precursor molecules need to be "up-converted" and liberated from their substituents to enable the build up of the graphene carbon lattice. In contrast to such elementary reactions on the substrate surface, larger molecular systems either can be cleaved according to parameters applied in a thermodynamically controlled CVD reaction, or, in case they exhibit a designed structure and substitution pattern, can lead to a precise bottom-up self-assembly of nanoribbon structures.[32,33]

**Morphological Aspects.** Typical SEM images are depicted in Figure 2. A rather homogeneous carbon film coverage is indicated, *e.g.*, for methane and pyridine in the presence of additional hydrogen in the gas phase [*cf.* Figure 2a,b], whereas without additional hydrogen, these deposits become rather inhomogeneous [*cf.* Figure 2d,e].

Interestingly, the CVD of precursors containing aliphatic $NO_2$- groups like nitromethane and nitroethane did not result in the formation of any detectable graphene [*cf.* Figure 2c] or carbon deposits irrespective of the presence of hydrogen, and unprecedented morphological changes resulting in a strongly etched surface were observed [*cf.* Figure 2c, 2d]. For nitroethane, *e.g.*, round hole structures in the Cu foil as depicted in Figure 2c,f were detected (similarly for nitromethane, *cf.* Supporting Information). The mass loss of copper during CVD (typically 1.6% reduction in case of CVD of nitromethane and nitroethane and 1.6–2.0% in the CVD of methane) is similar in both cases. The formation of the observed structures can be attributed to a yet unknown etchant species leading to a transport reaction and restructuring of the copper substrate surface.

**Raman Spectroscopy of the CVD Films.** The resulting films from the CVD experiments contain graphene, when the Raman spectra reveal the signature of the graphene 2D mode together with a G mode of appropriate line width. The 2D mode is only observed if a highly ordered carbon lattice is present in contrast to Raman spectra of nanoscale $sp^2$-type amorphous carbon showing only broad disordered (D) and graphitic (G) modes resulting from rather imperfect lattices. Carbon giving rise to these types of spectra reveals nanoscale graphene domains in contrast to a highly ordered mono- or multilayer graphene lattice with significant 2D contribution. Monolayer to few layer graphene can be discriminated according to the line width of the G and 2D modes. In our case, the line width indicates that few layer graphene is present, as also observed by the exfoliated TEM sample shown in Figure 8. The term graphene in this paper thus refers not exclusively to a monolayer, but to one or more 2D lattices of necessary perfection leading to the presence of a significant 2D contribution in the Raman spectra.[34]

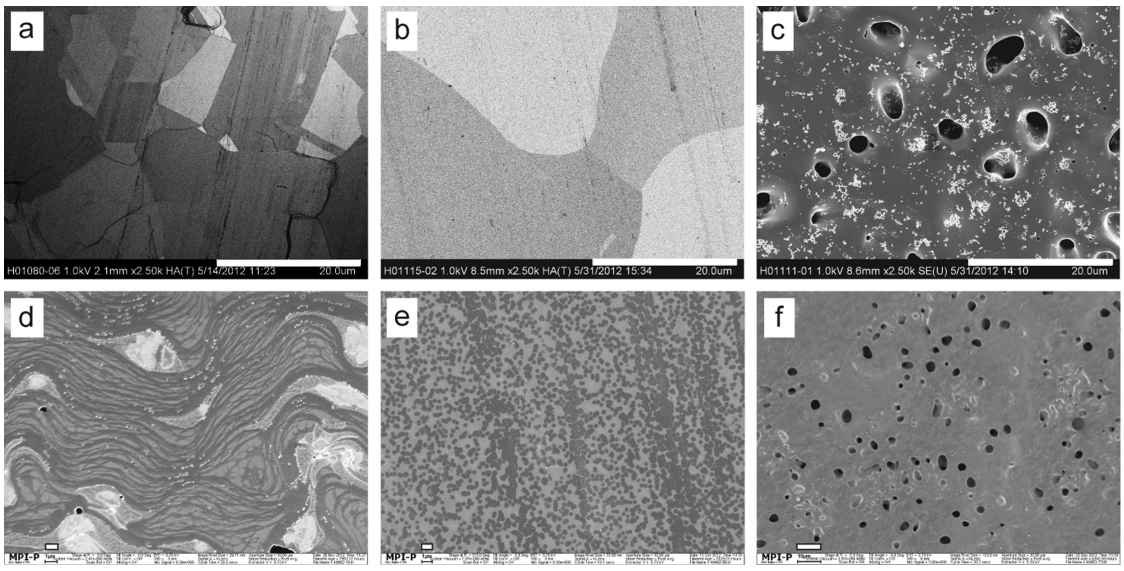


**Figure 2. SEM images of graphene, N-doped graphene, and carbon deposits on copper substrates obtained from different precursors: (a) methane, (b) pyridine, and (c) nitroethane [all with addition of hydrogen during CVD] and (d) methane, (e) pyridine, and (f) nitroethane [all without addition of hydrogen during CVD]. The scale bar is 20 $\mu$m for (a), (c), 300 $\mu$m for (b), 1 $\mu$m for (d,e), and 10 $\mu$m for (f). The SEM images for nitromethane are comparable to nitroethane and given in the Supporting Information.**

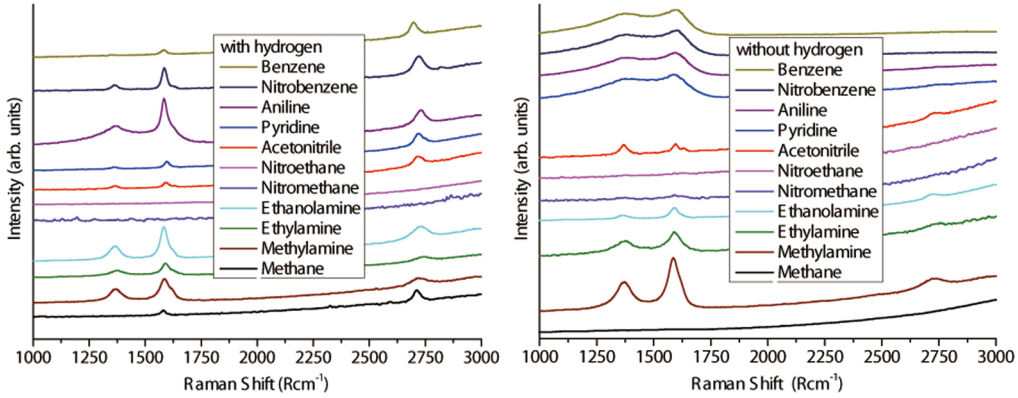


**Figure 3. Precursor and gas phase dependence of the Raman spectra of the CVD graphene/N-doped graphene/carbon films obtained at 1000 °C with additional hydrogen (left) and without additional hydrogen present during CVD (right).**

The Raman spectra of the CVD samples obtained with and without hydrogen (see Table 1, Figure 3, and Supporting Information) were measured directly on the copper foil. The quality of the graphene films can be evaluated using the ratio of the intensities of the G and 2D modes ($I_{2D}/I_G$) by a comparison of the resulting film quality of precursors with structurally related features and regarding the influence of the gas phase composition (*e.g.*, additional hydrogen content).

In this study, we commonly observe the D′ peak in carbon films obtained by CVD of nitrogen-containing precursors, which give rise to a 2D graphene signal. Since nitrogen atoms on graphene lattice positions are acting as defects, too, the more pronounced D′ peak appearance can be related to an incorporation of nitrogen. The presence of the D′ mode is obvious in films obtained from nitrogen-containing precursors like aliphatic amines, acetonitrile, pyridine, and aniline. The pronounced occurrence of the D′-peak in these films can be interpreted as an incorporation of nitrogen atoms into the graphene lattice on substitutional sites, in analogy to the Raman spectrum of nitrogen-doped graphene.[15,16]

**Graphene Quality As Per $I_{2D}/I_G$ Intensity.** If the graphene quality is rated by the ratio of the Raman G and 2D mode intensities ($I_{2D}/I_G$),[35] then the quality of the films decreases in the order of pyridine, acetonitrile, nitrobenzene, ethanolamine, ethylamine, aniline, and methylamine if additional hydrogen is present in the gas phase. Without hydrogen, significant contributions of 2D and G modes which indicate the presence of graphene were mainly identified for the precursors with $C_1$- and $C_2$- units. Films from acetonitrile reveal the highest value of the $I_{2D}/I_G$ ratio, whereas the films from aromatic precursors do not show any significant graphene signals.

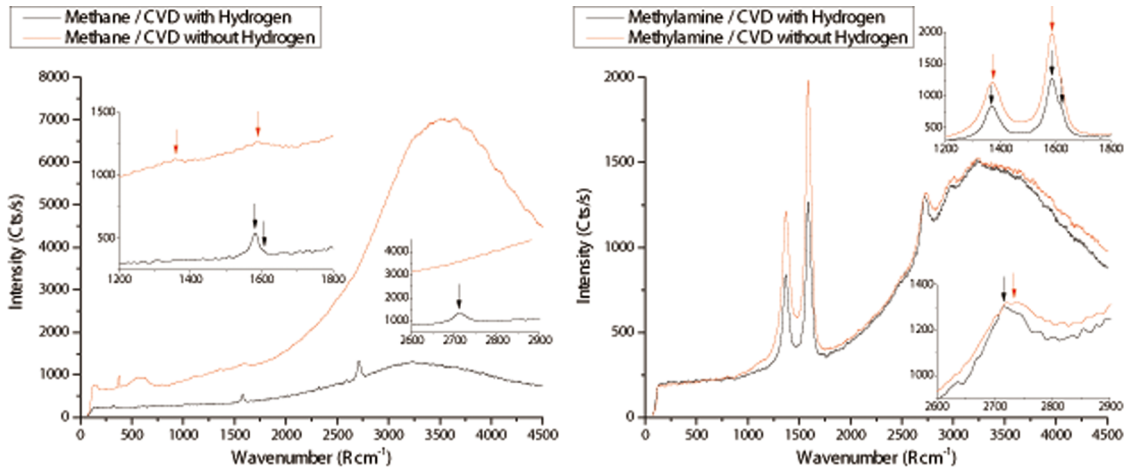


**Figure 4. Raman spectra indicating the formation of unstructured carbon without additional hydrogen or high quality graphene with additional hydrogen in the case of methane CVD (left). Direct formation of graphene in the case of methylamine CVD (right) even without addition of hydrogen reveals the precursor influence and the role of hydrogen on the CVD of (doped) graphene films. When comparing the total hydrogen content of the precursors during the neat decomposition of methane and methylamine, the actual hydrogen content of methylamine (16.19%) is even lower than that of methane (25.15%), but it still enables the formation of graphene during direct precursor CVD contrary to methane. This attributed to the weaker C−N bond energy leading to a more facile decay of the precursor and radical type gas phase species, *i.e.*, formation of methyl radicals and amine radicals.**

**Influence of the Gas Phase Composition.** The CVD of the precursors methylamine, ethylamine, ethanolamine, acetonitrile, pyridine, aniline, and nitrobenzene reveal significant differences from unsubstituted aliphatic (*e.g.*, methane) or aromatic systems (*e.g.*, benzene). A comparison of the most striking effects related to the presence of hydrogen as well as the precursor substitution is exemplified in Figure 4.

The formation of carbon films without significant contribution of high quality graphene is usually indicated by broad D and G modes without any sharp 2D modes of appropriate line width in the Raman spectra (Figure 3). This was observed for the direct CVD of methane without hydrogen, but also in the case of aromatic precursors like benzene, aniline, and pyridine. This finding might appear surprising since the latter precursors possess six-membered ring structures that formally resemble the graphene lattice. The formation of carbon films from these compounds is assumed to take place *via* defragmentation to a manifold of individual gas-phase species leading to an uncontrolled nucleation and growth of carbon films, although C−C bond formation between aromatic ring systems may also occur.

Graphene films were only formed in the presence of additional hydrogen during the CVD of methane and benzene, whereas, *e.g.*, methylamine does give rise to the presence of high quality graphene in the deposits irrespective of the presence of additional hydrogen. Besides the use of methylamine, the direct CVD of other nitrogen-containing precursors such as ethylamine, ethanolamine, acetonitrile, and aniline lead to the formation of graphene without additional hydrogen (*cf.* Supporting Information).

**Graphene Formation Considering Precursor Structures.** In this section, the graphene formation is screened according to the structural motifs of the precursors (Table 1). When comparing the graphene formation from ethylamine and acetonitrile, in the presence of hydrogen, the N-doped graphene obtained from acetonitrile reveals a higher quality than that from ethylamine. Also, the CVD of acetonitrile without additional hydrogen leads to the formation of carbon films with significant graphene structures. A similar effect, but less pronounced, is seen for films from ethylamine in the absence of hydrogen, thus indicating a better decay and graphene formation from acetonitrile. Ethylamine leads to higher-quality graphene films than methylamine, irrespective of the presence of hydrogen supporting the better suitability of $C_2$- type molecular fragments. Regarding $C_1$- type precursors, direct CVD of methane gives rise to unstructured carbon deposits, whereas the comparable decomposition of methylamine leads to a significant presence of graphene (*cf.* Figure 4). Also, for the precursors ethylamine, ethanolamine and acetonitrile, the formation of 2D mode is obvious, thus proving graphene formation by direct decomposition.

Oxygen from precursor molecules has in general no detrimental influence on the graphene formation and is easily eliminated in CVD reactions.[31] Therefore, it is reasoned that ethanolamine is also a suitable candidate for a more facile formation of $C_2$- type growth species compared to ethylamine, which is supported by the decay patterns of the EI-mass spectra.[36]

While comparing the CVD of aliphatic nitro compounds (nitromethane and nitroethane), both precursors fail to give any detectable carbon deposits. Regarding

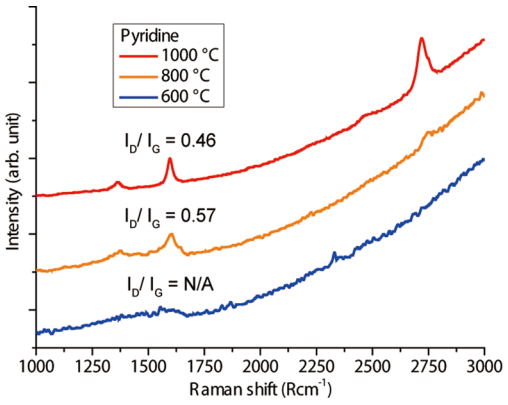


**Figure 5. Influence of deposition temperature on the Raman spectra of carbon films obtained from CVD of pyridine on copper in the presence of hydrogen: Formation of of N-doped graphene sheets at high temperatures.**

the CVD of aromatic precursors, pyridine produces high-quality N-doped graphene, and aniline and nitrobenzene form graphene-like structures of weaker quality in the presence of hydrogen. All (hetero)aromatic precursors do not furnish graphene during CVD conditions without additional hydrogen.

**Influence of the Deposition Temperature.** Since the CVD of pyridine in the presence of hydrogen gave rise to reasonable graphene film qualities, the CVD temperature influence on quality of the Raman spectra of films was studied as an example (Figure 5).

The structure of the deposits ranges from amorphous carbon (600 °C) *via* defect-rich (N-doped) graphene (800 °C) toward less defective (N-doped) graphene (1000 °C). The precursor decomposition and formation of solid carbon deposits requires different activation energies compared to the carbon network reconstruction, which finally results in the formation of high quality graphene structures from already formed carbon deposits. The precursor deposition at 600−800 °C leads to disordered carbon structures, whereas at higher temperatures, the thermodynamically controlled carbon network formation dominates the graphene formation (*cf.* Figure 6). Thus, the deposited materials are reconstructed toward the energetically more stable structure of perfect graphene (an effect related to the phase formation of solids by "Ostwald" ripening). The decomposition of nitrogen components is more pronounced at 1000 °C because intensity ratio of $I_D/I_G$ at 1000 °C is lower than that at 800 °C.

**TEM Characterization.** A high quality graphene film obtained from CVD of pyridine in the presence of hydrogen was transferred from the substrate and characterized with TEM (Figure 7). A sheet structure consisting of 2 layers with the layer distance of about 0.34 nm was observed. Electron diffraction patterns reveal double spots of 6-fold symmetry suggesting an N-doped graphene with a twisted double layer structure.[37]

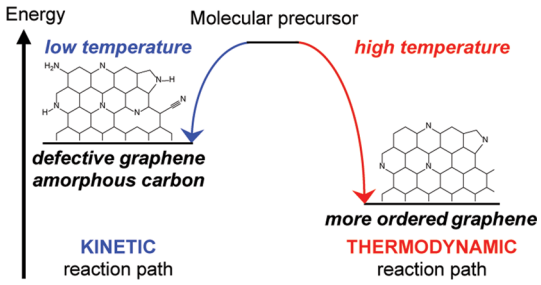


**Figure 6. Schematic representation of a kinetically and thermodynamically controlled reaction pathway for the formation of N-doped graphene. In a kinetically favored reaction, the structure is more defective with a higher Nitrogen content resulting from different functional groups, whereas for a thermodynamic controlled reaction, the graphene structure is more perfect with fewer heteroatoms and functional groups.**

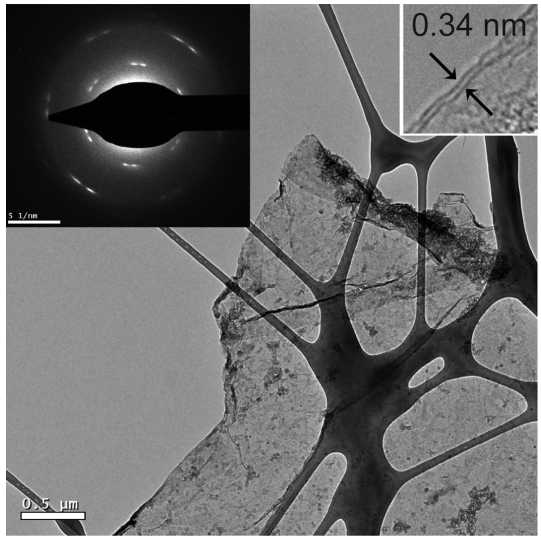


**Figure 7. TEM image of N-doped graphene sheets obtained from CVD of pyridine on copper with additional hydrogen after removal of the substrate. The insets display the selected electron diffraction pattern and the number of layers and thickness (0.34 nm).**

**Elemental Composition of the Films.** The chemical compositions of the films were investigated with XPS (*cf.* Figure 8 and Supporting Information).

The relative proportions of C, N, O, and of N bonding states were summarized in Table 2.

All samples reveal C1s as well as O1s signals. Standard graphene CVD for obtaining large transferable films is performed in either ambient conditions or at reduced pressure in a vacuum, but not in well controlled UHV conditions. Presently the literature offers no consistent XPS analysis of the as-prepared films addressing the presence of additional oxygen in the CVD films. The system leak rates and gas impurities, both usually not specified in the literature, can introduce oxygen, nitrogen, and water as the main contaminants from the air, which can influence the nucleation and growth mechanisms of the graphene formation and lead to unintentional N-doping.

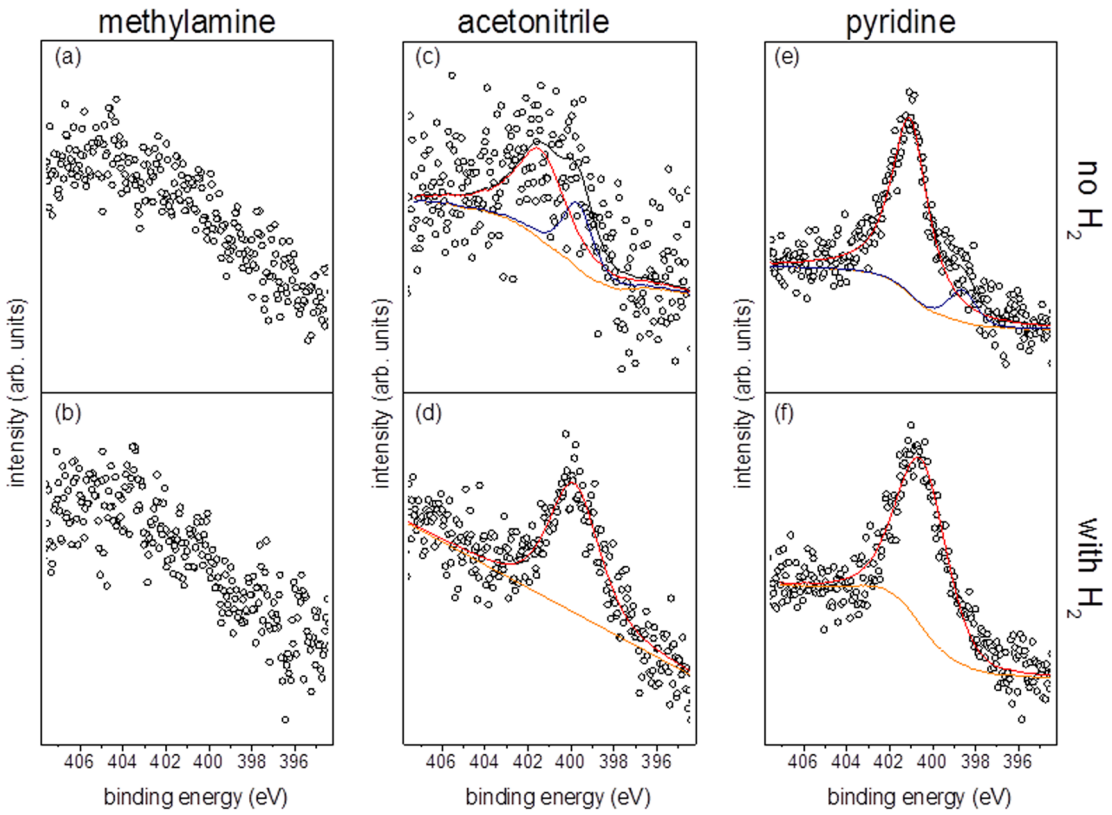


**Figure 8. XPS spectra of N1s emission of (N-doped) graphene films obtained from methylamine (a,b), acetonitrile (c,d), and pyridine (e,f) without or with additional hydrogen during CVD deposition, leading to a reduction of the pyridinic contribution.**

An addition of hydrogen during the film growth reduces the carbon content as well as the nitrogen content. The oxygen O1s content in the film is less strongly affected and cannot be suppressed beyond the detection limit by the hydrogen treatment. Surprisingly, the N1s content is low in the case of CVD of methylamine and other aliphatic amines, which indicates a predominant cleavage into carbon and nitrogen radical species in the gas phase. This is in accordance with the bond energies of the precursors.

The relative carbon content in films from aromatic precursors obtained by direct precursor CVD is generally higher, and the total carbon content of the films is increased for aliphatic amines, whereas the carbon content is lower for methane. This implicates more facile formation of radicals in case of the latter precursors, which can be considered as the responsible growth species for the film formation. The detectable amount of nitrogen is low in XPS, especially for aliphatic amines. This implies a separation of the precursors into mainly $C_xH_y$ and $N_aH_b$ gas-phase species with different sticking kinetics to the surface, resulting in a predominantly carbon deposition. Additional hydrogen presence during CVD leads to a decrease of the carbon as well as the nitrogen content and thus is acting as an etchant for *both* atomic species. Selected N1s signals are depicted in Figure 8. While the Raman

**TABLE 2. XPS Summary of the C/O/N Ratio of the Film Surfaces[a]**

| precursor | conditions | % C | % O | % N |
|---|---|---|---|---|
| methane $CH_4$ | no $H_2$ | 59.54 | 39.86 | 0.60 |
| | with $H_2$ | 45.04 | 54.96 | 0.00 |
| methylamine $CH_3-NH_2$ | no $H_2$ | 71.60 | 28.40 | 0.00 |
| | with $H_2$ | 78.10 | 21.90 | 0.00 |
| ethylamine $CH_3-CH_2-NH_2$ | no $H_2$ | 78.08 | 20.94 | 0.98 |
| | with $H_2$ | 73.66 | 26.34 | 0.00 |
| ethanolamine $HO-CH_2-CH_2-NH_2$ | no $H_2$ | 78.08 | 21.92 | 0.00 |
| | with $H_2$ | 56.44 | 42.86 | 0.70 |
| nitromethane $CH_3-NO_2$ | no $H_2$ | 60.03 | 39.65 | 0.32 |
| | with $H_2$ | 47.09 | 52.29 | 0.63 |
| nitroethane $CH_3-CH_2-NO_2$ | no $H_2$ | 47.59 | 51.89 | 0.52 |
| | with $H_2$ | 37.66 | 62.34 | 0.00 |
| acetonitrile $CH_3-CN$ | no $H_2$ | 69.34 | 30.54 | 0.12 |
| | with $H_2$ | 53.35 | 45.36 | 1.30 |
| pyridine $C_5H_4N$ | no $H_2$ | 83.59 | 13.78 | 2.63 |
| | with $H_2$ | 58.63 | 39.47 | 1.91 |
| aniline $C_6H_5-NH_2$ | no $H_2$ | 89.49 | 8.44 | 2.07 |
| | with $H_2$ | 89.44 | 9.57 | 1.00 |
| nitrobenzene $C_6H_5-NO_2$ | no $H_2$ | 90.37 | 8.61 | 1.02 |
| | with $H_2$ | 73.06 | 26.69 | 0.26 |
| benzene $C_6H_6$ | no $H_2$ | 86.63 | 13.16 | 0.21 |
| | with $H_2$ | 76.93 | 22.92 | 0.15 |

[a] Types of nitrogen atoms in the precursors: amine type (methylamine, ethylamine, ethanolamine, aniline), nitro type (nitromethane, nitroethane, nitrobenzene), nitrile type (acetonitrile), hetreoaromatic (pyridine).

**TABLE 3. Peak Positions and Linewidths (in $cm^{-1}$) of D, G, and D′ Bands and Intensity Ratios of D, G, D′, and 2D Peaks in the Raman Spectra (488 nm Excitation with 2 mW Power) Of Transferred Graphene Sheets on Glass**

| | D band/ line width | G band/ line width | D′ band/ line width | 2D band/ line width | $I_D/I_G$ | $I_{2D}/I_G$ | sheet resistance ($10^4$ Ohm/sq) | transparency (%) |
|---|---|---|---|---|---|---|---|---|
| graphene | — | 1583 | 1627 | 2690.5 | — | 2.9 | 0.36 | 98 |
| | — | 22 | 10 | 24 | | | | |
| ethylamine | 1364 | 1595 | 1627 | 2714 | 1.3 | 0.3 | 3.2 | 93 |
| | 32 | 25 | 10 | 28 | | | | |
| acetonitrile | 1359 | 1598 | 1631.5 | 2708.5 | 0.8 | 2.2 | 1.0 | 98 |
| | 16 | 14 | 10 | 25 | | | | |
| pyridine | 1353.5 | 1587 | 1624 | 2694.5 | 1.5 | 1.5 | 1.8 | 98 |
| | 28 | 20 | 13 | 25 | | | | |
| ethanolamine | 1351.5 | 1591 | 1627.5 | 2693.5 | 2.1 | 1.9 | 1.9 | 92 |
| | 16 | 20 | 10 | 28 | | | | |

spectra obtained after CVD of methylamine reveal the typical signature for N-doped graphene, the total nitrogen content is below the detection limit of the XPS analysis. Aliphatic amines thus have a tendency to directly increase the graphene formation irrespective of the amount of incorporated nitrogen.

**Optical and Electronic Characterization.** The exfoliated graphene and N-doped graphene sheets were transferred onto a glass substrate. The Raman spectroscopic data, sheet resistance, and optical transparencies of the films are summarized in Table 3. The Raman spectra of the N-doped graphene sheets obtained from pyridine, acetonitrile, and ethanolamine reveal high quality graphene indicating a successful transfer step. The sheet resistance of N-doped graphene is reported to be higher compared to graphene, which is explained by a n-type semiconductor behavior leading to a decrease in conductivity.[25] The values listed in Table 3 indicate good transparencies and high film qualities, and the transparency of these N-doped graphene films at 550 nm is comparable to that of undoped graphene films. Therefore, N-doped graphene created by various nitrogen-doped precursors demonstrates both high transparency and n-type transport properties, simultaneously.

## CONCLUSION

Precursors with different nitrogen-containing functional groups were used for the formation of nitrogen-doped graphene. The most striking difference is obvious from a direct comparison of CVD of methane and methylamine, which clearly indicates that not only the gas phase composition, but also the precursor chemistry has a significant influence on the graphene growth mechanisms. In general, small nitrogen-containing precursors like aliphatic amines or nitriles tend to form (nitrogen-doped) high quality CVD graphene without additional hydrogen in the gas phase, as indicated by the presence of the G and 2D modes in the Raman spectra. The presence of these moieties leads to a significant change in the growth kinetics and facilitates the formation of highly ordered graphene type carbon structures. This is a significant finding, and the effects resulting from the precursor substitution patterns and the influence of amine type nitrogen on the growth kinetics of graphene are obvious. In addition, the use of a precursor with both hydroxyl groups and amine groups (*e.g.*, ethanolamine) does not inhibit formation of graphene.

The presence of the D mode in the Raman spectra and the overall carbon content in the XPS measurements reveal that the direct precursor decomposition leads to the co-deposition of defective graphene structures and formation of non-$sp^2$-type carbon. The presence of additional hydrogen during CVD conditions decreases the carbon and the nitrogen content and acts as an etchant for *both* atomic species. Nevertheless the quality of the films can still be enhanced by subsequent optimization of the CVD parameters. The observed decay of the precursors is in accordance with their bond strengths. The reason for the enhanced quality of graphene type carbon can be seen in the more facile bond cleavage due to smaller single bond energies for C—O and C—N bonds as compared to C—H bonds.

Considering the standardized bond energies of the relevant groups (given in kJ/mol for single bonds: H—H 432, C—H 416, N—H 391, *C—N 305*, C—O 358, C—C 345, C—Cl 357; double bonds: C═N 616; triple bond: C≡N 892),[38] it is obvious that the C—N single bond energy is lowest in this series and can lead to a more facile radical formation in the gas phase in case of, *e.g.*, methylamine compared to methane.

Therefore, any functional groups enabling a more facile breakup of the precursors, *e.g.*, halides, are also considered feasible for a better carbon and graphene deposition from the gas phase. These findings are in accordance with the fact that precursors with C—N multiple bonds (*e.g.*, acetonitrile and pyridine) lead to higher nitrogen contents than aliphatic amines, as revealed by XPS in Figure 8. Furthermore, the Raman spectra of films originating from amines or nitrogen-containing precursors show a significant contribution of the D′ mode, which therefore can be attributed to a specific defect that is induced dominantly by

nitrogen-containing precursors. For aliphatic amines, which do not show any significant N1s content, the Raman spectra still reveal the same signature as reported for nitrogen-doped graphene, thus indicating a higher sensitivity for the Raman spectroscopic analysis.

Kinetic decay mechanisms dominate the nitrogen incorporation into the graphene lattice at lower temperatures, while a thermodynamic reaction pathway is favored at higher temperatures, and these aspects are also reflected in the resulting graphene qualities.

The key results of our finding (direct formation of graphene, Raman signature of N-doped graphene, little influence of additionally added hydrogen especially in the case of aliphatic amine precursors) lead to a new insight of the relevant gas phase species for graphene growth during CVD and open new parameter fields in the system. In addition, hydrogen in the gas phase also influences the nature of N1s signal structure and thus affects the doping.

Therefore, a detailed screening of small aliphatic and aromatic precursors with specific substitution patterns under controlled p, T- parameter regimes can enable the formation of doped and undoped graphene of superior quality.

## METHODS

Chemicals were purchased from commercial suppliers: methane (99.95%), pyridine (99.8%), acetonitrile (99.5%), methylamine (lecture bottle, 97%), ethylamine (97%), nitromethane (98.5%), nitrobenzene (99% extra pure), aniline (99%), benzene (99.5%) from Sigma-Aldrich; nitroethane (99%), Cu foils (25 $\mu$m thickness, 99.8%) from Alfa Aesar; ethanolamine (99%) from ROTH. Liquid precursors were dried and purified by standard distillation techniques prior to use.

N-Doped graphene films were prepared in a hot wall CVD setup comparable to other methods[39] with a modified precursor inlet system. Details are described in the Supporting Information. Cu foils (7 cm $\times$7 cm) were placed in a hot wall furnace inside a quartz tube. A typical CVD procedure was performed as follows: The system was evacuated, and the leak rate was tested. (leak rate: $<10^{-3}$ mbar/5 s). The leak rate also can give rise to the presence of oxygen in the CVD films. The system was flushed with hydrogen gas by maintaining a pressure of 1.5 mbar for cleaning the copper substrate. The tube was heated to 1000 °C (hydrogen flow 150 sccm at 1.5 mbar). After reaching the desired temperature, the molecular precursors were allowed to react for 20 min, respectively, with or without additional hydrogen flow [partial pressure of precursors in parentheses: methane (0.2 mbar), methylamine (3.0 mbar), ethylamine (3.0 mbar), ethanolamine (0.3 mbar), nitromethane (3.0 mbar), nitromethane (3.0 mbar), acetonitrile (3.0 mbar), pyridine (3.0 mbar), aniline (0.20 mbar), nitrobenzene (0.1 mbar), and benzene (1.0 mbar)]. After the exposure, the furnace was allowed to cool to room temperature. Experiments at different temperatures were employed similarly. The resulting CVD samples on Cu foils were coated with poly(methyl methacrylate) (PMMA) and then floated in dilute $Fe(NO_3)_3$ (0.05 g/mL). After dissolution of Cu, the PMMA-coated film was transferred onto a quartz ($SiO_2$) substrate. The residual PMMA was removed with acetone, and the remaining graphene film on quartz was washed with isopropyl alcohol.

Scanning electron microscopy (SEM) was performed with a Zeiss LEO 1530 Gemini at 1.0 keV and Hitachi SU8000 at 1.0 keV. The transmission electron microscopy (TEM) characterization was done using FEI Tecnai F20. X-ray photoelectron spectroscopy (XPS) was performed using a nonmonochromatic Al K$\alpha$ photon source (1486.6 eV) and a SPECS Phoibos 100 hemispherical energy analyzer. Graphitic carbon materials deposited on a Cu foil were fixed on a sample holder and introduced into the analysis chamber of a custom-made ultrahigh vacuum setup (base pressure at $10^{-10}$ mbar). The atomic sensitivity factors of the core levels were provided by SPECS. Raman spectra were measured with a BRUKER SENTERRA Spectrometer (488 nm, 2 mW, 200 ms accumulation time, 50 $\mu$m aperture, the spectra were analyzed with a Lorentzian fitting). The sheet resistance of transferred graphene films was measured by with a JANDEL micropositioning probe. The transparency of the graphene films on glass substrates was measured with a PERKIN ELMER Lambda 900 UV/vis/NIR spectrometer.

*Conflict of Interest:* The authors declare no competing financial interest.

*Acknowledgment.* This work was supported by the FP7 Advanced Grant AdG-2010 267160 "NANOGRAPH"; The Chemist's Way of Making and Utilizing Perfect Graphenes from the European Research Council and by the Marie-Curie Grant ITN-GENIUS (PITN-GA-2010-264694) and FP7-NMP-2010-SMALL-4 (HYMEC, PN 263073) from the European Commission. We thank Dr. I. Lieberwirth and G. Glaßer for TEM and SEM assistances.

*Supporting Information Available:* CVD parameters and Raman spectra. This material is available free of charge *via* the Internet at http://pubs.acs.org.

## REFERENCES AND NOTES

1. Boehm, H. P.; Clauss, A.; Fischer, G. O.; Hoffmann, U. Dünnste Kohlenstoff Folien. *Z. Naturforsch.* **1962**, *17 b*, 150–153.
2. Geim, A. K.; Novoselov, K. S. The Rise of Graphene. *Nat. Mater.* **2007**, *6*, 183–191.
3. Novoselov, K. S.; Fal'ko, V. I.; Colombo, L.; Gellert, P. R.; Schwab, M. G.; Kim, K. A Roadmap for Graphene. *Nature* **2012**, *490*, 192–200.
4. Novoselov, K. S. Nobel Lecture: Graphene: Materials in the Flatland. *Rev. Mod. Phys.* **2011**, *83*, 837–849.
5. Schwierz, F. S. F. Graphene Transistors. *Nat. Nanotechnol.* **2010**, *5*, 487–496.
6. Berger, C.; Song, Z. M.; Li, T. B.; Li, X. B.; Ogbazghi, A. Y.; Feng, R.; Dai, Z. T.; Marchenkov, A. N.; Conrad, E. H.; de Heer, W. A. Ultrathin Epitaxial Graphite: 2D Electron Gas Properties and a Route towards Graphene based Nanoelectronics. *J. Phys. Chem. B* **2004**, *108*, 19912–19916.
7. Wang, D. W.; Gentle, I. R.; Lu, G. Q. Enhanced Electrochemical Sensitivity of PtRh Electrodes coated with Nitrogen-Doped Graphene. *Electrochem. Commun.* **2010**, *12*, 1423–1427.
8. Wang, Y.; Shao, Y.; Matson, D. W.; Li, J.; Lin, Y. Nitrogen-Doped Graphene and Its Application in Electrochemical Biosensing. *ACS Nano* **2010**, *4*, 1790–1798.
9. Hou, J.; Shao, Y.; Ellis, M. W.; Moore, R. B.; Yi, B. Graphene-based Electrochemical Energy Conversion and Storage: Fuel Cells, Supercapacitors and Lithium Ion Batteries. *Phys. Chem. Chem. Phys.* **2011**, *13*, 15384–15402.
10. Pumera, M. Electrochemistry of Graphene: New Horizons for Sensing and Energy Storage. *Chem. Rec.* **2009**, *9*, 211–223.
11. Wang, Y.; Shi, Z.; Huang, Y.; Ma, Y.; Wang, C.; Chen, M.; Chen, Y. Supercapacitor Devices Based on Graphene Materials. *J. Phys. Chem. C* **2009**, *113*, 13103–13107.
12. Reddy, A. L. M.; Srivastava, A.; Gowda, S. R.; Gullapalli, H.; Dubey, M.; Ajayan, P. M. Synthesis Of Nitrogen-Doped Graphene Films For Lithium Battery Application. *ACS Nano* **2010**, *4*, 6337–6342.

13. Qu, L.; Liu, Y.; Baek, J.-B.; Dai, L. Nitrogen-Doped Graphene as Efficient Metal-Free Electrocatalyst for Oxygen Reduction in Fuel Cells. *ACS Nano* **2010**, *4*, 1321–1326.
14. Wang, X.; Zhi, L.; Muellen, K. Transparent, Conductive Graphene Electrodes for Dye-Sensitized Solar Cells. *Nano Lett.* **2008**, *8*, 323–327.
15. Terrones, H.; Lv, R.; Terrones, M.; Dresselhaus, M. S. The Role of Defects and Doping in 2D Graphene Sheets and 1D Nanoribbons. *Rep. Prog. Phys.* **2012**, *75*, 062501.
16. Lv, R.; Li, Q.; Botello-Mendez, A. R.; Hayashi, T.; Bei, W.; Berkdemir, A.; Hao, Q.; Elias, A. L.; Cruz-Silva, R.; Humberto R. Gutierrez, H. R.; *et al.* Nitrogen-Doped Graphene: Beyond Single Substitution and Enhanced Molecular Sensing. *Sci. Rep.* **2012**, *2*, 586.
17. Wang, H.; Maiyalagan, T.; Wang, X. Review on Recent Progress in Nitrogen-Doped Graphene: Synthesis, Characterization, and its Potential Applications. *ACS Catal.* **2012**, *2*, 781–794.
18. Endo, M.; Hayashi, T.; Hong, S.-W.; Enoki, T.; Dresselhaus, M. S. Scanning Tunneling Microscope Study of Boron-Doped Highly Oriented Pyrolytic Graphite. *J. Appl. Phys.* **2001**, *90*, 5670–5674.
19. Martins, T. B.; Miwa, R. H.; da Silva, A. J. R.; Fazzio, A. Electronic and Transport Properties of Boron-Doped Graphene Nanoribbons. *Phys. Rev. Lett.* **2007**, *98*, 196803.
20. Strelko, V. V.; Kuts, V. S.; Thrower, P. A. On the Mechanism of Possible Influence of Heteroatoms of Nitrogen, Boron and Phosphorus in a Carbon Matrix on the Catalytic Activity of Carbons in Electron Transfer Reactions. *Carbon* **2000**, *38*, 1499–1503.
21. Son, Y.-W.; Cohen, M. L.; Louie, S. G. Half-Metallic Graphene Nanoribbons. *Nature* **2006**, *444*, 347–349.
22. Li, X.; Wang, X.; Zhang, L.; Lee, S.; Dai, H. Chemically Derived, Ultrasmooth Graphene Nanoribbon Semiconductors. *Science* **2008**, *319*, 1229–1232.
23. Zhu, Y.; Murali, S.; Cai, W.; Li, X.; Suk, J. W.; Potts, J. R.; Ruoff, R. S. Graphene and Graphene Oxide: Synthesis, Properties, and Applications. *Adv. Mater.* **2010**, *22*, 3906–3924.
24. Dreyer, D. R.; Park, S.; Bielawski, C. W.; Ruoff, R. S. The Chemistry of Graphene Oxide. *Chem. Soc. Rev.* **2010**, *39*, 228–240.
25. Wei, D. C.; Liu, Y. Q.; Wang, Y.; Zhang, H. L.; Huang, L. P.; Yu, G. Synthesis of N-Doped Graphene by Chemical Vapor Deposition and Its Electrical Properties. *Nano Lett.* **2009**, *9*, 1752–1758.
26. Luo, Z.; Lim, S.; Tian, Z.; Shang, J.; Lai, L.; MacDonald, B.; Fu, C.; Shen, Z.; Yu, T.; Lin, J. Pyridinic N Doped Graphene: Synthesis, Electronic Structure, and Electrocatalytic Property. *J. Mater. Chem.* **2011**, *21*, 8038–8044.
27. Cui, T.; Lv, R.; Huang, Z. H.; Zhu, H.; Kang, F.; Wang, K.; Wu, D. Effect of Feed Rate on the Production of Nitrogen-Doped Graphene from Liquid Acetonitrile. *Carbon* **2012**, *50*, 3659–2665.
28. Terasawa, T.; Saiki, K. Synthesis of Nitrogen-Doped Graphene by Plasma-Enhanced Chemical Vapor Deposition *J. Appl. Phys.* **2012**, *51*, 055101.
29. Lin, Y.-C.; Lin, C.-Y.; Chiu, P.-W. Controllable Graphene N-Doping with Ammonia Plasma. *Appl. Phys. Lett.* **2010**, *96*, 133110.
30. Robertson, J.; Davis, C. A. Nitrogen Doping of Tetrahedral Amorphous Carbon. *Diamond Relat. Mater.* **1995**, *4*, 441–444.
31. Mueller, F.; Sachdev, H.; Huefner, S.; Pollard, A. J.; Perkins, E. W.; Russell, J. C.; Beton, P. H.; Gsell, S.; Fischer, M.; Schreck, M.; Stritzker, B. How Does Graphene Grow? Easy Access to Well-Ordered Graphene Films. *Small* **2009**, *5*, 2291–2296.
32. Chen, L.; Hernandez, Y.; Feng, X.; Müllen, K. From Nanographene and Graphene Nanoribbons to Graphene Sheets: Chemical Synthesis. *Angew. Chem., Int. Ed.* **2012**, *51*, 7640–7654.
33. Dössel, L.; Gherghel, L.; Feng, X.; Müllen, K. Graphene Nanoribbons by Chemists: Nanometer-Sized, Soluble, and Defect-Free. *Angew. Chem., Int. Ed.* **2011**, *50*, 2540–2543.
34. Ferrari, A. C. Raman Spectroscopy of Graphene and Graphite: Disorder, Electron−Phonon Coupling, Doping and Nonadiabatic Effects. *Solid State Commun.* **2007**, *143*, 47–57.
35. Ferrari, A. C.; Meyer, J. C.; Scardaci, V.; Casiraghi, C.; Lazzeri, M.; Mauri, F.; Piscanec, S.; Jiang, D.; Novoselov, K. S.; Roth, S.; Geim, A. K. Raman Spectrum of Graphene and Graphene Layers. *Phys. Rev. Lett.* **2006**, *97*, 187401.
36. Linstrom, P. J., Mallard, W. G., Eds.; *NIST Chemistry WebBook*, NIST Standard Reference Database Number 69; National Institute of Standards and Technology: Gaithersburg MD, 20899; http://webbook.nist.gov (retrieved August 19, 2013).
37. Ohta, T.; Beechem, T. E.; Robinson, J. T.; Kellogg, G. L. Long-Range Atomic Ordering and Variable Interlayer Interactions in two Overlapping Graphene Lattices with Stacking Misorientations. *Phys. Rev.* **2012**, *85*, 075415.
38. Holleman, A., Wiberg, E. *Lehrbuch der Anorganischen Chemie*; Wiberg, N., Ed.; de Gruyter: Berlin, 2007.
39. Li, X.; Magnuson, C. W.; Venugopal, A.; Tromp, R. M.; Hannon, J. B.; Vogel, E. M.; Colombo, L.; Ruoff, R. S. Large-Area Graphene Single Crystals Grown by Low-Pressure Chemical Vapor Deposition of Methane on Copper. *J. Am. Chem. Soc.* **2011**, *133*, 2816–2819.